photonics

MDPI

Article

67.5% Efficient InP-Based Laser Power Converters at 1470 nm at 77 K

Simon Fafard * and Denis Masson

Broadcom (Canada), Industrial Fiber Product Division, Ottawa, ON K1A 0R6, Canada; denis.masson@broadcom.com
* Correspondence: simon.fafard@broadcom.com

Abstract: Recent developments in long wavelength and cryogenic laser power converters have unlocked record performances in both areas. Here, devices for an optical input at ~1470 nm are studied for cryogenic applications, combining these cryogenic and long-wavelength attributes. Multijunction laser power converters are demonstrated to have a high-efficiency operation at 77 K. The photovoltaic-power-converting III-V semiconductor devices are designed with InGaAs-absorbing layers, here with 10 thin subcells (PT10), connected by transparent tunnel junctions. Unprecedented conversion efficiencies of up to 67.5% are measured at liquid nitrogen temperatures with an output power of P_{mpp} = 1.35 W at an average optical input intensity of ~62 W/cm^2. A remarkably low bandgap voltage offset value of W_{oc}~50 mV is obtained at an average optical input intensity of ~31 W/cm^2.

Keywords: optical power converters; laser power converters; power-over-fiber; power-beaming; photovoltaic multijunctions; galvanic isolation; InGaAs; InP; bandgap voltage offset (W_{oc})

1. Introduction

Optical power converter (OPC) device developments are derived from the different requirements of optical wireless power transmission (OWPT) and power-over-fiber (PoF) applications. For that purpose, vertical multijunction laser power converters (LPCs) continue to be implemented with the aim of enabling key optically powered probes, sensors, and electronic subsystem capabilities [1–4]. As shown in Figure 1, such LPCs are optimally designed for various spectral, power, and temperature ranges. They have been demonstrated to be stable and reliable for different power-over-fiber or power-beaming applications for the industrial operating range from −40 °C to 85 °C. Power-demanding, remote, isolated, and backup applications are, therefore, readily satisfied with vertical multijunction LPC products, which are distinctively capable of producing watts of output power.

From the optical source perspective, the 808 nm laser diodes are ubiquitous in many commercial applications and have also recently been used with multijunction LPCs for space applications or scientific experiments requiring cryogenic temperatures [2]. For example, liquid argon or the liquid xenon time-projection chamber are of great interest for fundamental neutrino experiments and detection, dark matter research, or for cosmic-muon data recording [5–7].

Multijunction designs are also particularly critical for the longer-wavelength spectral ranges, and new LPCs for the 1450–1550 nm spectral range have been commercialized [4]. However, reports on the cryogenic performance of PV devices with substantial conversion efficiencies in that spectral range are lacking.

This study is focused on combining the cryogenic and long-wavelength attributes of recently developed OPCs. We further develop and characterize vertical multijunction OPCs with 10 thin subcells (PT10), designed for an input wavelength at ~1470 nm at cryogenic temperatures. The semiconductor structure is based on the vertical epitaxial heterostructure architecture (VEHSA) design [1]. These cryogenic 1470 nm LPCs are utilizing InGaAs absorbers lattice-matched to InP: PT10-InGaAs/InP. Fabricated chips with

check for updates

Citation: Fafard, S.; Masson, D. 67.5% Efficient InP-Based Laser Power Converters at 1470 nm at 77 K. *Photonics* **2024**, *11*, 130. https://doi.org/10.3390/photonics11020130

Received: 5 January 2024
Revised: 25 January 2024
Accepted: 29 January 2024
Published: 30 January 2024

Copyright: © 2024 by the authors. Licensee MDPI, Basel, Switzerland. This article is an open access article distributed under the terms and conditions of the Creative Commons Attribution (CC BY) license (https://creativecommons.org/licenses/by/4.0/).

an area of ~0.032 cm^2 have been packaged in Broadcom's *Regular Power* format with an FC optical connector. The key performance parameters are obtained on a small assembly lot, with the devices measured at 77 K by immersion in liquid nitrogen.

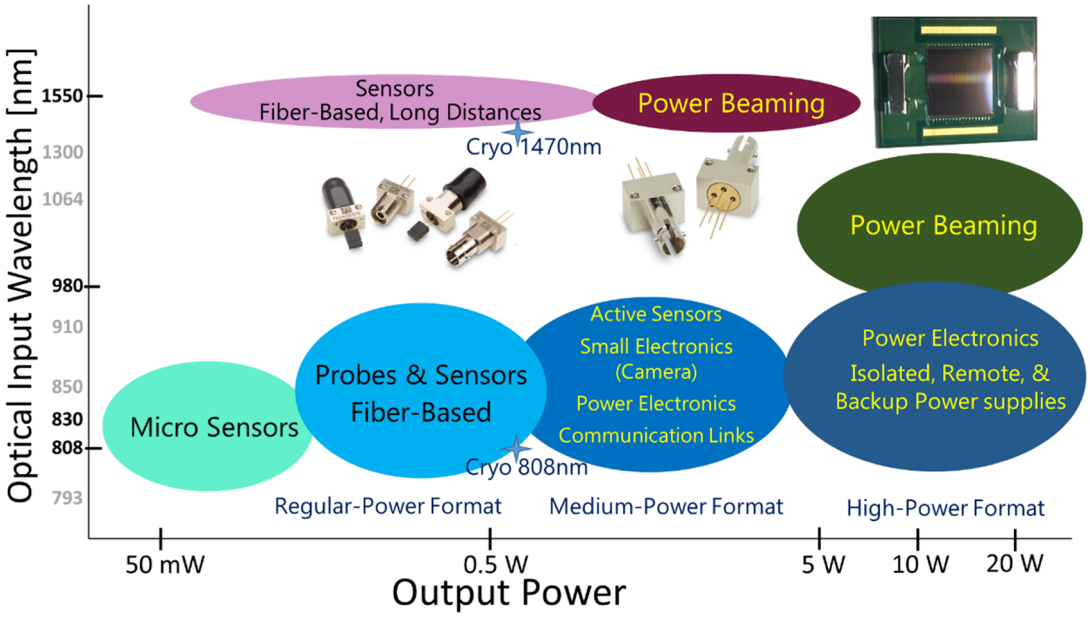


Figure 1. Illustration of the various OWPT applications, organized according to the OPC's output power (horizontal axis—log scale) and the wavelength of operation (vertical axis—not to scale). The updated chart includes the cryogenic applications at 808 nm and 1470 nm based on the *Regular Power* OPCs: blue star symbols. Adapted from ref. [1], Copyright 2021 author(s), licensed under a Creative Commons Attribution (CC BY) license.

2. Materials and Methods

The PT10-InGaAs/InP heterostructure is based on the previously described VEHSA design [1]. A schematic of the corresponding structure is depicted in Figure 2a. As is customary, the Beer–Lambert law is used to determine the thicknesses of the individual InGaAs subcells, with the target of having each subcell absorb ~1/10 of the incident light, for a wavelength of ~1470 nm, at an operating temperature of ~77 K. Consequently, to realize the required photocurrent-matching condition, the subcells have increasing thicknesses from the top subcell (thinnest) toward the bottom subcell (thickest), as illustrated in Figure 2a. In this study, a total absorber thickness of 3700 nm was used for the sum of all subcells, and the corresponding absorption profile is sketched in Figure 2b. For the ideal current-matched conditions, we evaluate that, nominally, the absorption at 77 K would be ~97% of the input beam at 1470 nm, with 9.7% being absorbed in each subcell.

The methodology for applying the Beer–Lambert approach has been described previously [1] and no corrections were implemented in the present study for photon coupling and recycling effects. It should be noted that no detailed InGaAs iso-cell characterizations were carried out to accurately optimize the heterostructure's current-matching at 77 K. Furthermore, methods have now been put forward based on machine learning and genetic algorithm to improve the optimization of the individual thicknesses [8,9]. Such models suggest that the evaluation using the Beer–Lambert model might underestimate the required thickness of the first subcells. In practice, it should therefore be expected that the subcells will not be fully current-matched and that further performance improvements can readily be obtained with additional iterations and/or with careful device modelling.

Overall, the PT10 is designed with 10 semiconductor photovoltaic (PV) subcells, which are interconnected with optically transparent tunnel junctions, as represented in Figure 2. Each individual subcell comprises an n-type emitter and a p-type base (i.e., n on p configuration). The tunnel junctions are made to be transparent to the input beam,

utilizing AlGaInAs alloys that are lattice-matched to InP. The epitaxial layers were grown using commercial production Aixtron Metal Organic Chemical Vapor Deposition (MOCVD) reactors.

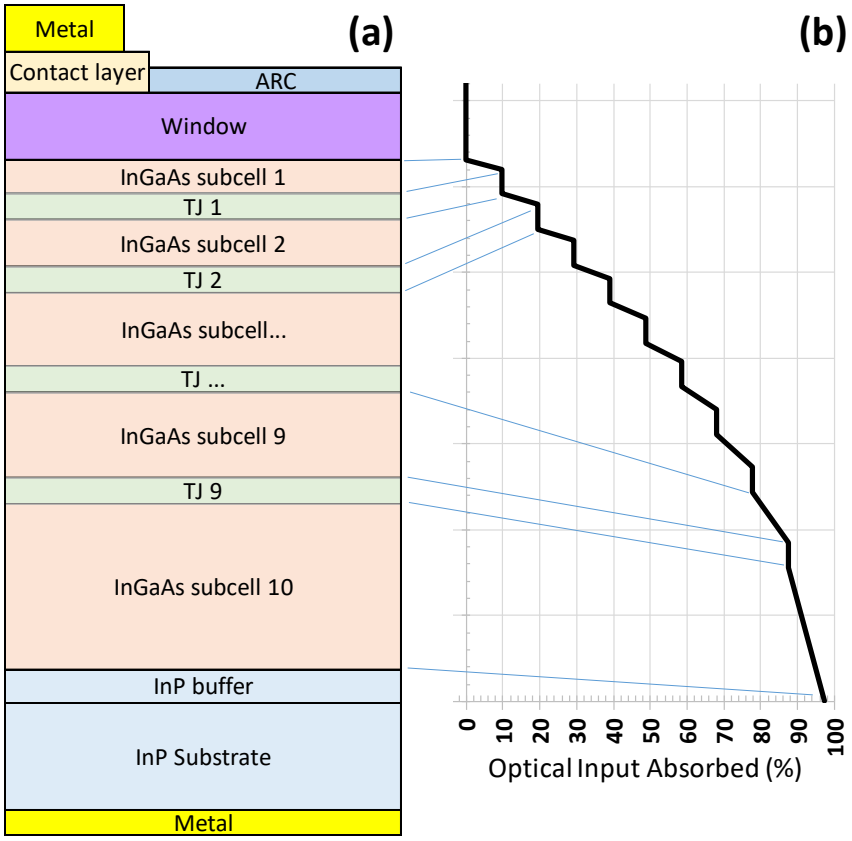


Figure 2. Schematic of the PT10-InGaAs/InP vertical epitaxial heterostructure architecture (VEHSA design) devices prepared with 10 InGaAs subcells and separated by tunnel junction (TJ), depicted in (**a**), and corresponding absorption profile of the optical input in (**b**).

For this study, the PT10-InGaAs/InP epitaxial wafers were fabricated into chips with an area of 0.032 cm^2. Over 1500 devices were fabricated in chips, including standard blanket back-metallization, front ohmic contacts, and antireflection coatings (ARC) constructed from layers of Al_2O_3 and TiO_2. The ARC typically reduces the reflectivity (R) of the incident beam to R < 4% for the spectral range of interest. All devices were tested using dark I-V measurements and a high level of chip uniformity was assessed from these dark I-V tests. An assembly lot of 75 devices was then processed into packages incorporating an optical fiber connector. These 75 PT10 devices were packaged in Broadcom's *Regular Power* housing, equipped with an FC optical connector [1]. The 75 chips of this assembly lot were selected to sample an area from one wafer, covering about two rows of chips from one edge of the wafer to the opposite edge, passing though the central area of the wafer.

For the performance measurements, the I-V characteristics were acquired using a Keithley 2601B source-meter in four-wire probing mode. A fiber-coupled laser diode emitting at ~1470 nm was used for the optical source [10]. This is manufactured by BWT with a numerical aperture of NA ~0.22, using a multi-mode fiber core diameter of 400 µm and cladding of 440 µm. The optical input is therefore obtained from a connectorized fiber pigtail, with a length of about 2 m. For most of the I-V measurements, the fiber-coupled laser was connected to the packaged PT10 and directly immersed in liquid nitrogen to obtain measurements at 77 K. In such a configuration, the optical connector and a fraction of the length of the laser pigtail are within the liquid nitrogen. Liquid nitrogen is, for all practical purposes, transparent near 1470 nm. It has an index of refraction of n ~1.2,

compared to air, with n ~1.0. Consequently, the slightly denser medium can help the transmission of light from the fiber tip to the device by, at most, a relative ~3%. The quoted efficiency refers to the measured device output power divided by the laser input power and includes the small benefit from the presence of the liquid nitrogen.

For variable temperature measurements, either the device was allowed to warm up after the liquid nitrogen was all evaporated, or a liquid nitrogen cryostat was used, equipped with a standard 1 kOhms resistance temperature detector (RTD) to directly measure the device temperature. Quick I-V scans were used to avoid significant chip heating or temperature drifts between the measurements.

3. Results

Figure 3 shows the data obtained from the small assembly lot measured at 77 K by liquid nitrogen immersion. As shown in Figure 3a, tight distributions were obtained with average output voltages of V_{oc}~7.52 V for the open circuit voltage and V_{mpp}~6.92 V for the voltage at the maximum power point. From the histogram of Figure 3b, the corresponding average conversion efficiency was Eff = 66.3%. Furthermore, as shown on the updated *Power Converter Performance Chart* in Figure 4, conversion efficiencies of up to Eff = 67.5% were obtained for an output power of P_{mpp} = 1.35 W at an input wavelength near 1470 nm: new data point (53).

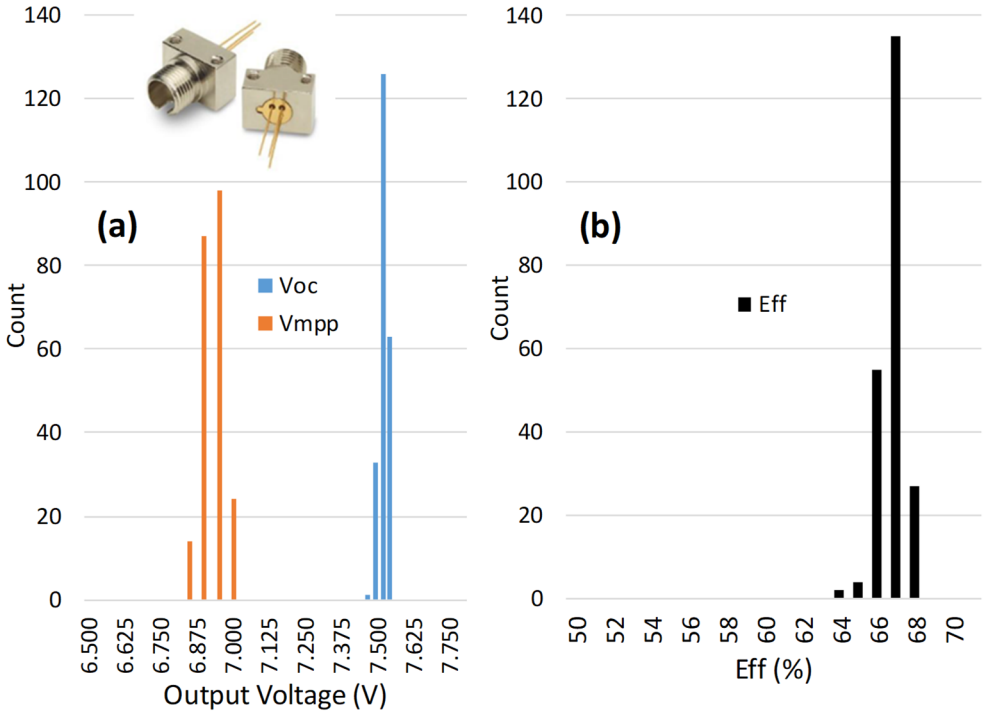


Figure 3. Example of histogram for the output voltage for regular-power OPCs with ~1470 nm optical inputs between 1.0 and 2.0 Watts, measured at 77 K on a lot of 75 devices. Output voltage shown in (**a**) and conversion efficiency shown in (**b**).

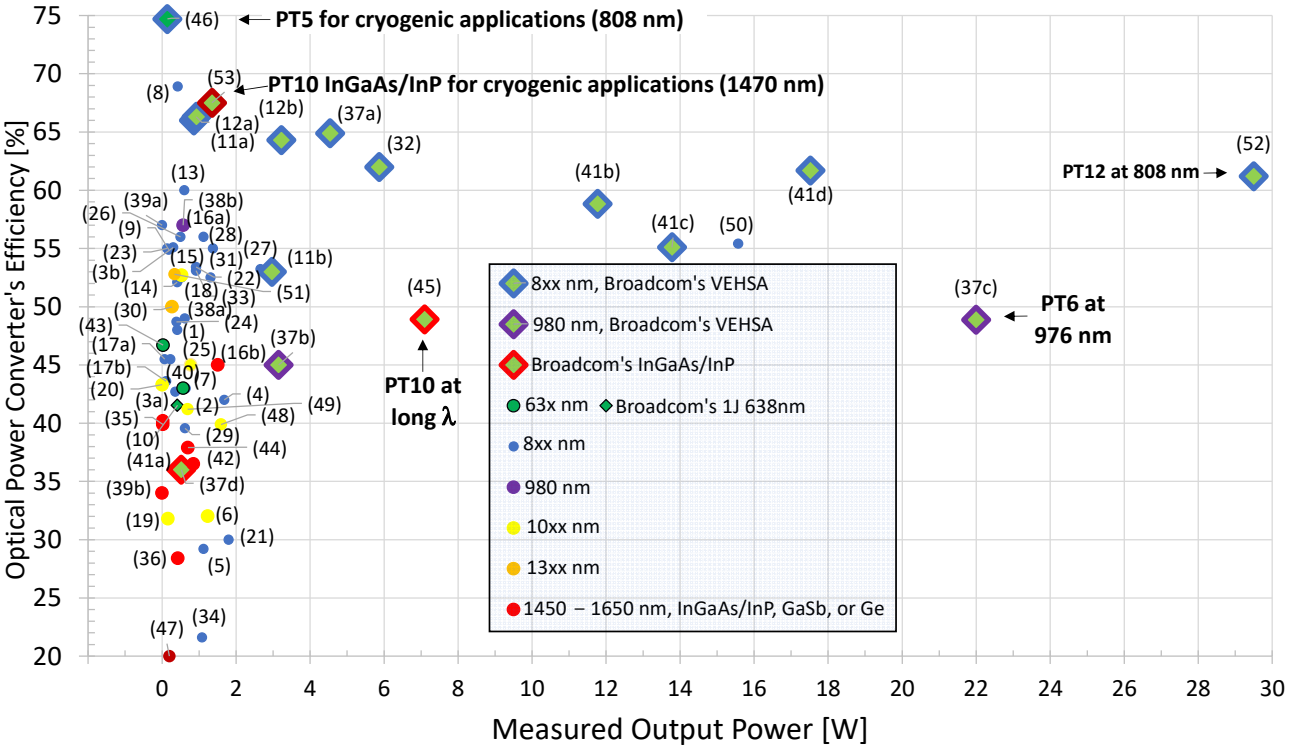


Figure 4. Updated *Power Converter Performance Chart* [1,3], including PT10-InGaAs/InP results of this study, shown with data point (53). Broadcom's vertical multi-junction data are represented by diamond-shaped symbols. Details for data points (1)–(52) are found in Reference [3] and references therein (i.e., see the matching numbers in the reference section of Reference [3]). Updated from S. Fafard and D. P. Masson, J. Applied Physics 130, 160901 (2021) and Photonics 10, 940 (2023). Copyright 2021–2023 author(s), licensed under a Creative Commons Attribution (CC BY) license.

As shown in Figure 5a, for this assembly lot, the output power P_{mpp} was found to have a measured linear slope of Eff ~66% with the optical input power. Negligible deviations from linear regression were obtained for optical input powers up to 3 W, corresponding to an average optical intensity of 93.8 W/cm^2. A regression coefficient of $R^2 = 0.9999$ was obtained for the lot of 75 packaged devices in Figure 3. The sample lot of 75 devices was measured for the *Regular Power* range of input powers, reaching up to 2.0 W (blue crosses data points), but one sample was measured for an extended range of up to 3.0 W (black circles represent data points). Extensive reliability data were previously obtained with the *Regular Power* form factor for operation at up to 2.0 W of optical input power [1], but the data in Figure 5 suggest that stable operation at an even higher input power might be possible, particularly for cryogenic conditions. Figure 5b shows that the corresponding average conversion efficiency remains at Eff ~66 +/− 0.5% in the range between 0.25 W and 3.0 W of input power. For an ideal diode with no resistive losses at a constant junction temperature, the efficiency would continue to increase as the optical input power increases. However, in the present case, V_{oc} reaches a maximum value near 1 W of input power, and then progressively decreases by 58 mV as the input power reaches 3 W. The latter suggests that the junction temperature effectively increases by a few Kelvins for higher optical input powers. As a net result, the measured efficiency remains relatively flat with the input power [11].

The measured record cryogenic conversion efficiency for InP-based long wavelength OPCs is approaching the previously obtained cryogenic conversion efficiencies, measured at 808 nm with the GaAs-based OPCs: data point (46) in Figure 4. Furthermore, the PT10-InGaAs/InP has the advantage that the optical input wavelength (~1470 nm) is well past the cutoff threshold of sensitive silicon-based detectors like photomultipliers (SiPM), which are often used in such cryogenic applications.

Therefore, in addition to being compatible with common electronics requirements and having an optical input that is well-suited to propagation over long distances, these new OPCs can also be more advantageous for cryogenic applications.

We have also shown recently, using GaAs-based PT12, data point (52) in Figure 4, that the multijunction LPC devices can be very tolerant to beam non-uniformity, partial illumination, or beam displacement variations [3]. The latter attribute is particularly important for power-beaming applications, which would also apply to long-wavelength OPCs operating at cryogenic temperatures (e.g., for space applications).

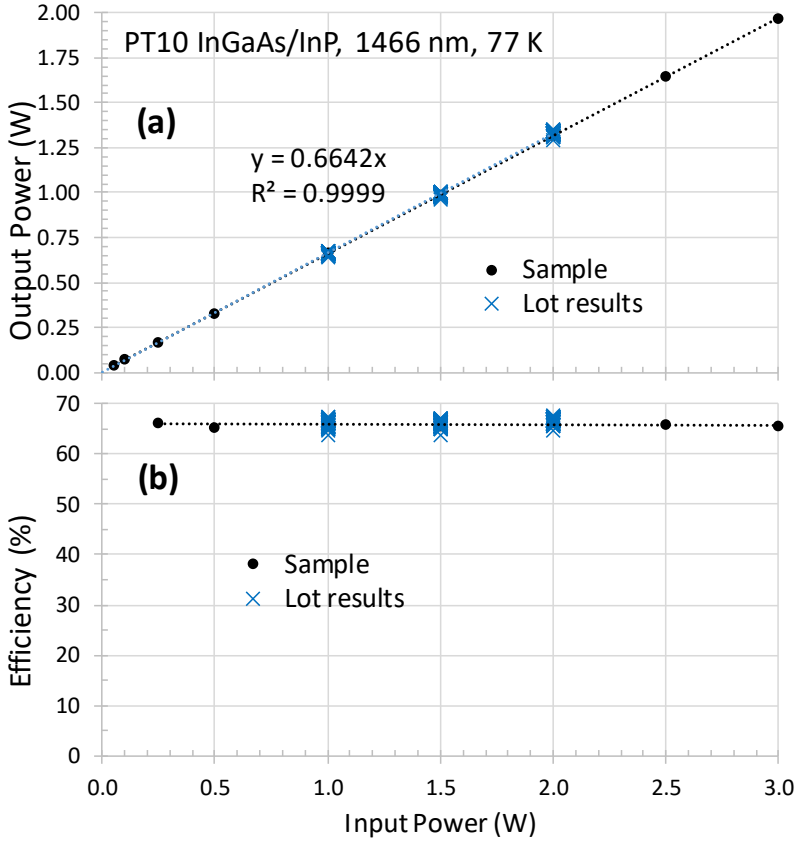


Figure 5. Performance of PT10 InGaAs/InP OPCs for cryogenic temperature applications. Optical input power dependence of the output power (P_{mpp}) in (**a**) and of the PV conversion efficiency in (**b**).

The temperature dependence of the PT10-InGaAs/InP key properties is analyzed in in Figure 6 for an optical input power of ~1 W (average optical input intensity of ~31 W/cm^2). The output voltage is shown in the upper part of Figure 6. A 0.032 cm^2 chip was mounted onto a cryostat equipped with a 1 kiloOhm RTD and used to directly assess the temperature of the device while the PT10-InGaAs/InP is warming up from liquid nitrogen temperature to room temperature. The V_{oc} varies linearly with temperature, with a slope of −10.9 mV/K, as obtained from the linear regression for temperatures higher than about −175 °C (R^2 = 0.997); see the black curve in Figure 6. Similarly, V_{mpp} also varies linearly with temperature with a slope of −12.5 mV/K, as obtained from the corresponding linear regression (R^2 = 0.999); see the blue curve in Figure 6. The data for the lot measured at 77 K are also included in Figure 6 for optical input powers between 1 W and 2 W. Evidently, the increase in output voltage saturates for temperatures colder than about −175 °C.

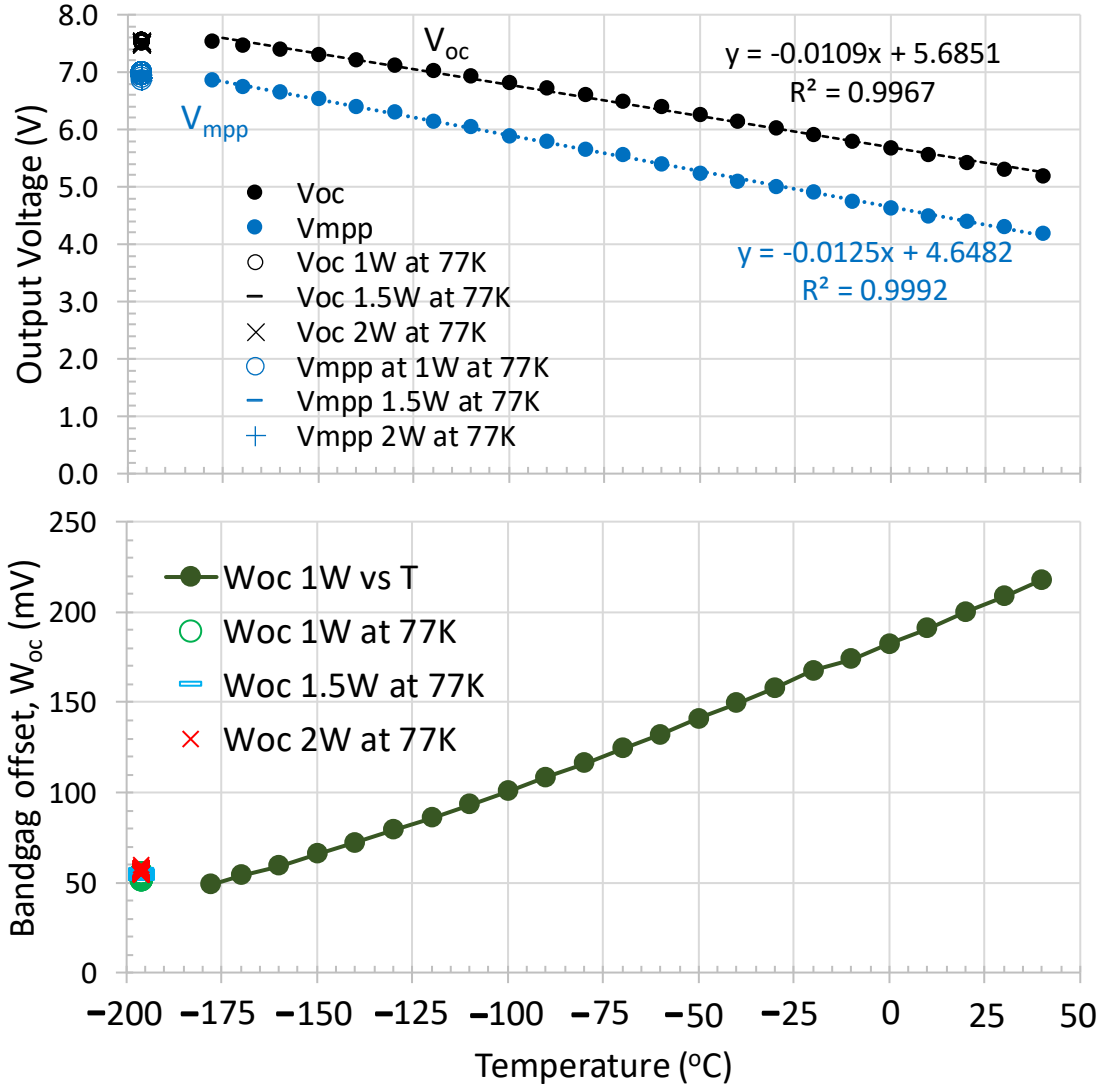


Figure 6. Temperature dependence of the output voltage (**top**), V_{oc} in black and V_{mpp} in blue, and the bandgap voltage offset, W_{oc}, (**bottom** in green) for an optical input at ~1470 nm with a power of ~1 W. The measured 77 K data for the lot of 75 devices are also included for optical input powers between 1 W and 2 W.

Remarkably, the open-circuit voltage (V_{oc}) reaches high values at cryogenic temperatures: average values at 77 K of V_{oc} = 7.516 V, with the maximum value measured for the lot of V_{oc} = 7.547 V. A V_{oc} of 7.547 V corresponds to an average voltage of 0.7547 V per subcell, yielding a bandgap voltage offset value of W_{oc} = 51.6 mV, where $W_{oc} = (E_g/q) - V_{oc}$, with E_g being the bandgap energy and q serving as the electronic charge. For photovoltaic devices, smaller bandgap voltage offset values are well-known to be indicative of the high quality of the semiconductor material (i.e., lower W_{oc} values are very much desirable) [12–15].

Here, E_g is about 0.806 eV for InGaAs that are lattice-matched to InP at 77 K, using the bandgap for a temperature T to be $E_g(T) = 0.814 - 4.906 \times 10^{-4}\ T^2/(T + 301)$ eV, as shown by Yu et al. [16]. The measured temperature dependence of W_{oc} for the PT10-InGaAs/InP OPCs is shown via the green curve at the bottom of Figure 6: the bandgap offset value decreases from about 200 mV at 20 °C to the best value of W_{oc}~50 mV at cryogenic temperatures for an optical input of ~31 W/cm^2. As can also be seen for the W_{oc} values obtained from the 77 K data points of the devices in the lot, no further decrease in the W_{oc} values is observed for temperatures colder than about −175 °C.

For the GaAs-based cryogenic PT5 OPCs with five subcells, a bandgap voltage offset value of W_{oc} = 71 mV was measured at an average optical input intensity of ~7 W/cm^2, around 77 K. It was evaluated that, for an average optical input intensity of ~62 W/cm^2, such GaAs-based PT5 would be expected to have a W_{oc} value of 57 mV [2]. Therefore, the W_{oc} values obtained with the InP-based PT10 appear to be lower by a few mV than the ones obtained with the GaAs-based cryogenic PT5.

4. Discussion

At 77 K, the average conversion efficiency for the assembly lot was found to be Eff = 66.3%, with average maximum power point parameters of V_{mpp} = 6.925 V and I_{mpp} = 144 mA. These values correspond to average external quantum efficiencies of EQE_{sc} = 86.9% and EQE_{mpp} = 81.0% for the short-circuit and maximum power point, respectively.

For the GaAs-based cryogenic PT5 OPCs, a better current-matching condition was obtained in the range of 150 K < T < 180 K, with EQE_{mpp} values reaching about 90% at the maximum power point at an input wavelength of 808 nm [2]. Therefore, it is reasonable to assume that, similarly, EQE_{mpp} values of about 90% could also be obtained with better optimized, but realistic, conditions for the InP-based PT10 OPCs. The latter would be expected to provide conversion efficiencies of Eff = 73.7%. A conversion efficiency of Eff ~75% would require improving the EQE_{mpp} to ~91.7%, while keeping W_{oc} and the diode ideality factors the same. Such EQE improvements will most likely be achieved by further reducing the mismatch in the subcell's photocurrents while maintaining the W_{oc} value near 50 mV.

For the GaAs-based cryogenic OPCs, an 808 nm optical input wavelength is about 27 meV in energy above the GaAs bandgap at 77 K. The small energy difference above the bandgap is ideal to ensure a large enough absorption coefficient value while maintaining the low thermalization losses from the photocarriers excited above the absorber bandgap. Similarly, for the InP-based cryogenic OPCs, a 1470 nm optical input wavelength is about 37 meV in energy above the InGaAs bandgap at 77 K, and practically ideal.

The PoF applications requiring operation in liquid cryogen could benefit from the PT10-InGaAs/InP OPCs because they have the advantage that the optical input wavelength is well past the cutoff threshold of sensitive sensors like SiPM. In such configurations, the OPC and the input fiber can be directly immersed in liquid nitrogen or liquid argon. From our testing of different fiber types in immersed liquid nitrogen, we found that bare optical fibers with only a thin polyimide protective coating (no jacket) are preferred to minimize transmission losses in the fiber under cryogenic conditions [17]. It should be noted that bare polyimide-coated optical fibers are readily commercially available and have good mechanically integrity. Moreover, the response of high-sensitivity SiPM devices is expected to be unaffected by residual light at significantly longer wavelengths than the band-edge of the silicon semiconductor bandgap.

5. Conclusions

In this study, multijunction laser power converters were demonstrated for high-efficiency operation under cryogenic conditions for a long-wavelength optical input at around 1470 nm. The photovoltaic-power-converting III-V semiconductor devices were designed with 10 thin subcells comprising InGaAs-absorbing layers connected by transparent AlInGaAs tunnel junctions.

Conversion efficiencies of up to 67.5% were obtained at liquid nitrogen temperatures with an output power of P_{mpp} = 1.35 W at an average optical input intensity of ~62 W/cm^2. At an average optical input intensity of ~93 W/cm^2, an electrical output power of 2 W was demonstrated with a conversion efficiency of 65.7%. A low bandgap voltage offset value of W_{oc}~50 mV was obtained at an average optical input intensity of ~31 W/cm^2. Small bandgap voltage offset values are indicative of an efficient photocarrier extraction (typically associated with high-quality semiconductor material). For a multijunction architecture, the thinner PV subcells further facilitate the photocarrier extraction for a given photocarrier

lifetime; therefore, the multijunction design can potentially help to obtain low W_{oc} values. Importantly, low operating temperatures have been shown to be a major factor in achieving low W_{oc} values, which is also consistent with the higher photocarrier lifetimes observed at low temperatures.

While research on laser power converter devices continues to progress in many groups [18–37], our present study has expanded the possibilities for stable and reliable power-over-fiber or power-beaming devices that are obtained using vertical multijunction power converters. The multijunction design enables practical optimal loads and tailored output voltages. Such devices can be used for remote and galvanically isolated power deployment in harsh operating conditions, including cryogenic environments.

We observed that the transmission at wavelengths in the range of 1470 nm in bare polyimide-coated optical fibers is substantially unaffected by immersing the fiber in liquid nitrogen; therefore, light leakage must be minimal. In contrast, we found that the light leakage at 808 nm in various types of fibers immersed in liquid nitrogen can readily be measured (with infrared camera and even with the naked eye), and significant transmission losses are often obtained with only a few meters of fiber length. Such light leakage at 808 nm can certainly affect the high-sensitivity SiPM devices. Therefore, the 1470 nm prospect presented by the high-efficiency cryogenic OPCs of the present study, which represent a key improvement in applications requiring low noise levels.

Broadcom has released products for the 800–830 nm, the 960–990 nm, and the 1450–1550 nm spectral ranges. Both GaAs-based and InP-based LPCs have now been developed for potential cryogenic, high-sensitivity, low-noise applications [5–7,38,39].

Author Contributions: Conceptualization, S.F. and D.M.; methodology, S.F. and D.M.; software, S.F. and D.M.; validation, S.F. and D.M.; formal analysis, S.F. and D.M.; investigation, S.F. and D.M.; data curation, S.F. and D.M.; writing—original draft preparation S.F.; writing—review and editing S.F. and D.M.; visualization, S.F.; project administration, S.F. and D.M.; funding acquisition, S.F. and D.M. All authors have read and agreed to the published version of the manuscript.

Funding: This research received no external funding.

Institutional Review Board Statement: Not applicable.

Informed Consent Statement: Not applicable.

Data Availability Statement: The data that support the findings of this study are available from the corresponding author upon reasonable request.

Conflicts of Interest: The authors declare no particular conflicts of interest, but it should be noted that the authors are employed by Broadcom, a company that manufactures and sells semiconductor components, including power converter devices.

References

1. Fafard, S.; Masson, D.P. Perspective on photovoltaic optical power converters. *J. Appl. Phys.* **2021**, *130*, 160901. [CrossRef]
2. Fafard, S.; Masson, D.P. 74.7% Efficient GaAs-Based Laser Power Converters at 808 nm at 150 K. *Photonics* **2022**, *9*, 579. [CrossRef]
3. Fafard, S.; Masson, D.P. Vertical Multi-Junction Laser Power Converters with 61% Efficiency at 30 W Output Power and with Tolerance to Beam Non-Uniformity, Partial Illumination, and Beam Displacement. *Photonics* **2023**, *10*, 940. [CrossRef]
4. Fafard, S.; Masson, D.P. High-Efficiency and High-Power Multijunction InGaAs/InP Photovoltaic Laser Power Converters for 1470 nm. *Photonics* **2022**, *9*, 438. [CrossRef]
5. Delgado, M.; Gutiérrez, R.M.; Fuentes, F. Liquid argon photodetection systems for neutrino detectors: A minireview. *J. Phys. Conf. Ser.* **2020**, *1672*, 012009. [CrossRef]
6. Brizzolari, C.; Carniti, P.; Cattadori, C.; Cristaldo, E.; de la Torre Rojo, A.; Delgado, M.; Falcone, A.; Francis, K.; Gallice, N.; Gotti, C.; et al. Cryogenic front-end amplifier design for large SiPM arrays in the DUNE FD1-HD photon detection system. *J. Instrum.* **2022**, *17*, P11017. [CrossRef]
7. Temples, D.J.; McLaughlin, J.; Bargemann, J.; Baxter, D.; Cottle, A.; Dahl, C.E.; Lippincott, W.H.; Monte, A.; Phelan, J. Measurement of charge and light yields for Xe 127 L-shell electron captures in liquid xenon. *Phys. Rev. D* **2021**, *104*, 112001. [CrossRef]
8. Cicic, S.; Tomic, S. Automated design of multi junction solar cells by genetic approach: Reaching the >50% efficiency target. *Sol. Energy Mater. Sol. Cells* **2018**, *181*, 30–37. [CrossRef]

9. Čičić, S.; Tomić, S. Genetic algorithm designed high efficiency laser power converters based on the vertical epitaxial heterostructure architecture. *Sol. Energy Mater. Sol. Cells* **2019**, *200*, 109878. [CrossRef]
10. A BWT Beijing Ltd. Laser Diode Was Used as the ~1470 nm Source. Available online: https://www.bwt-bj.com/en/product/ (accessed on 4 January 2024).
11. Geisz, J.F.; Friedman, D.J.; Steiner, M.A.; France, R.M.; Song, T. Operando Temperature Measurements of Photovoltaic Laser Power Converter Devices Under Continuous High-Intensity Illumination. *IEEE J. Photovolt.* **2023**, *13*, 808–813. [CrossRef]
12. Gonzalo, A.; Stanojević, L.; Utrilla, A.D.; Reyes, D.F.; Braza, V.; Marrón, D.F.; Ben, T.; González, D.; Hierro, A.; Guzman, A.; et al. Open circuit voltage recovery in GaAsSbN-based solar cells: Role of deep N-related radiative states. *Sol. Energy Mater. Sol. Cells* **2019**, *200*, 109949. [CrossRef]
13. Jain, N.; Schulte, K.L.; Geisz, J.F.; Friedman, D.J.; France, R.M.; Perl, E.E.; Norman, A.G.; Guthrey, H.L.; Steiner, M.A. High-efficiency inverted metamorphic 1.7/1.1 eV GaInAsP/GaInAs dual-junction solar cells. *Appl. Phys. Lett.* **2018**, *112*, 053905. [CrossRef]
14. Friedman, D.J.; Geisz, J.F.; Kurtz, S.R.; Olson, J.M. 1-eV solar cells with GaInNAs active layer. *J. Cryst. Growth* **1998**, *195*, 409–415. [CrossRef]
15. Helmers, H.; Franke, A.; Lackner, D.; Höhn, O.; Predan, F.; Dimroth, F. 51% efficient photonic power converters for O-band wavelengths around 1310 nm. In Proceedings of the 2020 47th IEEE Photovoltaic Specialists Conference (PVSC), Calgary, AB, Canada, 15 June–21 August 2020; pp. 2471–2474.
16. Yu, P.W.; Kuphal, E. Photoluminescence of Mn- and un-doped Ga0.47In0.53As on InP. *Solid State Commun.* **1984**, *49*, 907–910. [CrossRef]
17. Lindholm, E.A.; Stolov, A.A.; Dyer, R.S.; Slyman, B.; Burgess, D. Reliability of optical fibers in a cryogenic environment. In Proceedings of the Fiber Optic Sensors and Applications VI, Orlando, FL, USA, 13–17 April 2009; SPIE: Bellingham, WA, USA, 2009; Volume 7316, pp. 258–263.
18. Helmers, H.; Lopez, E.; Höhn, O.; Lackner, D.; Schön, J.; Schauerte, M.; Schachtner, M.; Dimroth, F.; Bett, A.W. 68.9% Efficient GaAs-Based Photonic Power Conversion Enabled by Photon Recycling and Optical Resonance. *Phys. Status Solidi (RRL) Rapid Res. Lett.* **2021**, *15*, 2100113. [CrossRef]
19. Algora, C.; García, I.; Delgado, M.; Peña, R.; Vázquez, C.; Hinojosa, M.; Rey-Stolle, I. Beaming power: Photovoltaic laser power converters for power-by-light. *Joule* **2022**, *6*, 340–368. [CrossRef]
20. Mukherjee, J.; Jarvis, S.; Perren, M.; Sweeney, S.J. Efficiency limits of laser power converters for optical power transfer applications. *J. Phys. D Appl. Phys.* **2013**, *46*, 264006. [CrossRef]
21. Putra, E.P.; Theivindran, R.; Hasnul, H.; Lee, H.J.; Ker, P.J.; Jamaludin, Z.; Awang, R.; Yusof, F.A.M. Technology update on patent and development trend of power over fiber: A critical review and future prospects. *J. Photonics Energy* **2023**, *13*, 011001. [CrossRef]
22. Wang, A.-C.; Yin, J.-J.; Yu, S.-Z.; Sun, Y.-R.; Dong, J.-R. Origins of the short circuit current of a current mismatched multijunction photovoltaic cell considering subcell reverse breakdown. *Opt. Express* **2023**, *31*, 14482–14494. [CrossRef] [PubMed]
23. Sanmartín, P.; Almonacid, F.; Ceballos, M.A.; García-Loureiro, A.; Fernández, E.F. Wide-bandgap III-V materials for high efficiency air and underwater optical photovoltaic power transmission. *Sol. Energy Mater. Sol. Cells* **2024**, *266*, 112662. [CrossRef]
24. Beattie, M.N.; Valdivia, C.E.; Wilkins, M.M.; Zamiri, M.; Kaller, K.L.C.; Tam, M.C.; Kim, H.S.; Krich, J.J.; Wasilewski, Z.R.; Hinzer, K. High current density tunnel diodes for multi-junction photovoltaic devices on InP substrates. *Appl. Phys. Lett.* **2021**, *118*, 062101. [CrossRef]
25. Fafard, S.; Masson, D. Onset of Quantum-Confined Stark Effects in Multijunction Photovoltaic Laser Power Converters Designed with Thin Subcells. *Photonics* **2023**, *10*, 1243. [CrossRef]
26. Khvostikov, V.P.; Sorokina, S.V.; Khvostikova, O.A.; Nakhimovich, M.V.; Shvarts, Z. Ge-Based Photovoltaic Laser-Power Converters. *IEEE J. Photovolt.* **2023**, *13*, 254–259. [CrossRef]
27. Kalyuzhnyy, N.A.; Malevskaya, A.V.; Mintairov, S.A.; Mintairov, M.A.; Nakhimovich, M.V.; Salii, R.A.; Shvarts, M.Z.; Andreev, V.M. Photovoltaic AlGaAs/GaAs devices for conversion of high-power density laser (800–860 nm) radiation. *Sol. Energy Mater. Sol. Cells* **2023**, *262*, 112551. [CrossRef]
28. Kurooka, K.; Honda, T.; Komazawa, Y.; Warigaya, R.; Uchida, S. A 46.7% efficient GaInP photonic power converter under high-power 638 nm laser uniform irradiation of 1.5 W cm^{-2}. Appl. *Phys. Express* **2022**, *15*, 062003. [CrossRef]
29. Zhou, Y.; Guan, C.; Lv, H.; Zhang, Y.; Zhou, R.; Chu, W.; Lv, P.; Qin, H.; Li, S.; Li, X. Design and Research of Laser Power Converter (LPC) for Passive Optical Fiber Audio Transmission System Terminal. *Photonics* **2023**, *10*, 1257. [CrossRef]
30. Gou, Y.; Zhu, L.; Mou, Z.; Chen, Y.; Cheng, Y.; Wang, J.; Yang, H.; Deng, G. InP-based tunnel junctions for ultra-high concentration photovoltaics. *Opt. Express* **2024**, *32*, 408–414. [CrossRef]
31. Shi, L.; Sun, C.; Liu, Y.; Liu, K.; Zhang, W.; Wu, Y.; Guo, H.; Sun, Q. A novel method of determining bias lights for spectral response measurement of GaAs multi-junction laser power converters and its applications. *Sol. Energy Mater. Sol. Cells* **2024**, *266*, 112661. [CrossRef]
32. Zheng, Y.; Zhang, G.; Huan, Z.; Zhang, Y.; Yuan, G.; Li, Q.; Ding, G.; Lv, Z.; Ni, W.; Shao, Y.; et al. Wireless laser power transmission: Recent progress and future challenges. *Space Sol. Power Wirel. Transm.* 2024, in press. [CrossRef]
33. Huang, J.; Sun, Y.; Zhao, Y.; Yu, S.; Dong, J.; Xue, J.; Xue, C.; Wang, J.; Lu, Y.; Ding, Y. Four-junction AlGaAs/GaAs laser power converter. *J. Semicond.* **2018**, *39*, 044003. [CrossRef]

34. Jomen, R.; Tanaka, F.; Akiba, T.; Ikeda, M.; Kiryu, K.; Matsushita, M.; Maenaka, H.; Dai, P.; Lu, S.; Uchida, S. Conversion efficiencies of single-junction III–V solar cells based on InGaP, GaAs, InGaAsP, and InGaAs for laser wireless power transmission. *Jpn. J. Appl. Phys.* **2018**, *57*, 08RD12. [CrossRef]
35. Martinek, P.; Prajzler, V. Power over fiber using a large core fiber and laser operating at 976 nm with 10 W power. *Opt. Fiber Technol.* **2023**, *80*, 103404. [CrossRef]
36. Höhn, O.; Walker, A.W.; Bett, A.W.; Helmers, H. Optimal laser wavelength for efficient laser power converter operation over temperature. *Appl. Phys. Lett.* **2016**, *108*, 241104. [CrossRef]
37. Ahnood, A.; Ndabakuranye, J.P.; Li, S.; Kavehei, O.; Prawer, S. Miniature power and data transceiver based on multimodal operation of a single photovoltaic device. *Eng. Res. Express* **2020**, *2*, 015036. [CrossRef]
38. Abud, A.A.; Abi, B.; Acciarri, R.; Acero, M.A.; Adames, M.R.; Adamov, G.; Adamowski, M.; Adams, D.; Adinolfi, M.; Aduszkiewicz, A.; et al. Scintillation light detection in the 6-m drift-length ProtoDUNE Dual Phase liquid argon TPC. *Eur. Phys. J. C* **2022**, *82*, 618. [CrossRef]
39. Acerbi, F.; Paternoster, G.; Merzi, S.; Zorzi, N.; Gola, A. Nuv and vuv sensitive silicon photomultipliers technologies optimized for operation at cryogenic temperatures. *Nucl. Instrum. Methods Phys. Res. Sect. A Accel. Spectrometers Detect. Assoc. Equip.* **2023**, *1046*, 167683. [CrossRef]

Disclaimer/Publisher's Note: The statements, opinions and data contained in all publications are solely those of the individual author(s) and contributor(s) and not of MDPI and/or the editor(s). MDPI and/or the editor(s) disclaim responsibility for any injury to people or property resulting from any ideas, methods, instructions or products referred to in the content.